JOURNAL OF Applied Polymer SCIENCE

Simultaneously improving tensile strength and toughness of melt-spun β-nucleated isotactic polypropylene fibers

Zhongzhu Liu, Guoqiang Zheng, Kun Dai, Chuntai Liu, Changyu Shen
College of Materials Science and Engineering, the Key Laboratory of Advanced Materials Processing and Mold of Ministry of Education, Zhengzhou University, Zhengzhou 450001, People's Republic of China
Correspondence to: G. Zheng (E-mail: gqzheng@zzu.edu.cn) and C.Liu (E-mail: ctliu@zzu.edu.cn)

ABSTRACT: Polymer processing methods generally play a crucial role in determining the development of microstructure in the fabricated product. In this study, isotactic polypropylene (iPP) melt containing 0.05 wt % β-nucleating agent (β-NA) was extruded via a melt flow rate indicator. The molten extrudate was stretched into a fiber upon various take-up velocities (TVs). The microstructures of the fiber were investigated by differential scanning calorimeter, two-dimensional wide-angle X-ray diffraction, and small-angle X-ray scattering. Also, its tensile properties (including tensile strength, modulus, elongation at break, and toughness) were measured by tensile test. Interestingly, the tensile strength (135.0 MPa) of a melt-spun β-nucleated iPP fiber fabricated at 400 cm/min was enhanced by 115.2%, compared with that (62.7 MPa) prepared at 100 cm/min, with a considerable increment in toughness (from 661 to 853 MJ/m^3). The enhancement mechanism for tensile properties was discussed based on the microstructures. This work offers a simple approach to prepare β-nucleated iPP fibers with excellent strength and toughness. © 2016 Wiley Periodicals, Inc. J. Appl. Polym. Sci. **2016**, *133*, 43454.

KEYWORDS: crystallization; extrusion; fibers; polypropylene; structure–property relations

Received 12 October 2015; accepted 20 January 2016
DOI: 10.1002/app.43454

INTRODUCTION

Isotactic polypropylene (iPP) is a widely used and versatile commodity polymer, owing to its numerous advantages, such as low density, easy processing, recyclability, and excellent mechanical performances. It is a typical polymorphic plastic with at least three basic crystalline forms,[1,2] such as α-crystal (monoclinic), β-crystal (trigonal),[3,4] or γ-crystal (orthorhombic).[5] It can also form a mesomorphic structure,[6] which is often described as a smectic or paracrystalline phase. Among them, compared with common α-crystal, the β-crystal shows some unique characteristics such as improved toughness, so it has received considerable attention for academic interests and industrial applications.[7–10] Nevertheless, it is thermodynamically metastable and difficult to be obtained under common crystallization conditions.[9,11,12] Generally, the addition of β-nucleating agent (β-NA) is the most effective and accessible method to obtain a high content of β-crystal.[13,14] The mechanisms of β nucleation is as follows: it is reported that β-NA has strong nucleation ability and can present the solid state at 200 °C,[14,15] while the iPP has been completely molten at that temperature. Therefore, the β-NA can act as heterogeneous nuclei in the iPP melt. When the iPP melt containing β-NA was cooled from the molten state, the iPP can crystallize on such surface of heterogeneous nuclei, thus leading to the formation of β-crystal. In other words, β-crystal grows epitaxially on the β-NA.[16]

It is well known that shear and stretching generally exist in common polymer processing (i.e., injection molding, film blowing, and fiber spinning). Although stretching has an effect similar to that of shear on the promotion of crystallization, there are some differences, for example, stretching is much more effective in inducing chain extension.[17] Moreover, it has been established that stretching can not only facilitate the orientation and crystallization process of semi-crystalline polymers but also induce some interesting crystalline morphologies (e.g., shish-kebab) which can profoundly enhance final properties of the shaped products.[11,18,19]

As for the iPP fibers fabricated by melt-spinning, it has been studied since the early 1930s and it still continues to be of interest up to now.[1,20–25] It has been reported that the crystalline structure and resulting properties of melt-spun fibers are highly dependent on the spinning conditions, for example, take-up velocity (TV) and extrusion temperature.[20,21] Moreover, Lu and Spruiell[22] and Misra *et al.*[1] demonstrated that spinnability, resulting microstructures and properties are affected by both weight average molecular weight and polydispersity of iPP. It was found that, at given spinning conditions and resin MFR,

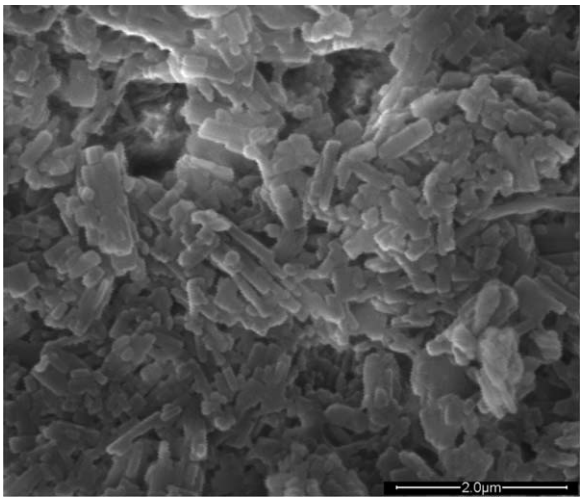

Figure 1. SEM micrograph for raw rare earth β-NA.

broadening the molecular weight distribution (increasing the polydispersity) produces an increase in crystallinity, tensile modulus, and elongation-to-break. Furthermore, Lu and Spruiell[23] also found that, when PP filaments are spun under relatively low stress and TV conditions, changing the crystallization kinetics can produce profound effects on the structure and properties of them. The structure–property relationship of the melt-spun polypropylene/whisker composite fibers was recently investigated by Gao *et al.*[25] The results showed that two different interfacial crystalline structures were observed by adopting two drawn ratios: shish-calabash structure at low drawn ratio and transcrystalline structure at high one. Meanwhile, compared with composite fibers obtained at low drawn ratio, remarkable reinforcement of that prepared at high drawn ratio was realized. Moreover, in the β-nucleated iPP samples prepared by melt-stretching, the change tendency of β-crystal structure upon stretching ratio has been systematically investigated in our previous study.[10] Unfortunately, the relationship between crystalline structure and mechanical properties was not further discussed in our aforementioned works. In a word, many studies have investigated the crystalline structures of melt-spun iPP fibers, but few of them systematically investigated the combined effect of various TVs and β-NA on crystalline structure and the relevant mechanical properties.

The objective of this study is to investigate the relationship between microstructures and tensile properties of the melt-spun β-nucleated iPP fibers prepared upon various TVs. It is very interesting to find that the combined effects of increasing TV and addition of β-NA simultaneously enhance the tensile strength and toughness in melt-spun β-nucleated iPP fibers.

EXPERIMENTAL

Materials

Commercial iPP (T30S) was bought from Dushanzi Petroleum Chemical Co. (Xinjiang, China), with a melt flow index (MFI) of 3.0 g/10 min (230 °C, 2.16 kg). Its $\bar{M}_w$, $\bar{M}_n$, and $\bar{M}_w/\bar{M}_n$ are 39.9 × 10^4 g/mol, 8.67 × 10^4 g/mol and 4.6, respectively. The rare earth β-NA was kindly supplied by Guangdong Winner Functional Materials Co., Ltd. β-NA is a heteronuclear dimetal complex of lanthanum and calcium with some specific ligands. Its general formula is $Ca_xLa_{1-x}(LIG1)_m(LIG2)_n$, where x and $1-x$ are the proportions of Ca^{2+} and La^{3+} ions in the complex, while LIG1 and LIG2 are, respectively, a dicarboxylic acid and amide-type ligand with coordination number of m and n.[26] The diameter of a single raw β-NA crystal is tens of nanometers, and the length is generally less than 1 μm. The detailed morphology of β-NA is shown in Figure 1.

Sample Preparation

The β-NA (0.05 wt %) was dry mixed with iPP in a valve bag and then melt mixed in a Haake internal mixer (Haake Polylab System-Rheomex 252P series). After pelletizing and drying, the mixture was melt-spun into fibers at 200 °C using a melt flow rate indicator with a die diameter 2.095 ± 0.005 mm. All the melt-spun β-nucleated iPP fibers were air-cooled and collected under tension by a home-made take-up device (see Figure 2). Four TVs (i.e., the linear speed of the take-up roller) were adopted: 100, 200, 300, and 400 cm/min.

Characterizations

Single-Fiber Tensile Test. The tensile experiments were carried out on a SUNS Universal tensile testing machine (UTM2203, Shenzhen Suns Technology Stock Co., Ltd, China) with a 100*N* load cell. The crosshead speed was 50 mm/min and the temperature was about 25 °C. All fibers were tested with a gauge length of 20 mm. The reported values were calculated as averages of at least five specimens for the fiber fabricated at a given TV.

Differential Scanning Calorimetry (DSC). The melting characteristics of the melt-spun β-nucleated iPP fibers were studied by DSC (TA Instruments, DSC-2920). The DSC furnace was purged with nitrogen during the measurement. The weight of each specimen was about 5–10 mg. The samples were heated from room temperature to 200 °C at a heating rate of 10 °C/min.

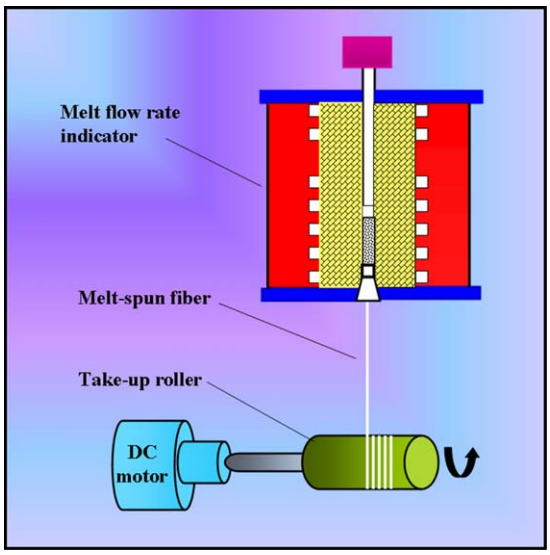

Figure 2. Schematic diagram for the melt-spinning of β-nucleated iPP fibers using melt flow rate indicator. [Color figure can be viewed in the online issue, which is available at wileyonlinelibrary.com.]

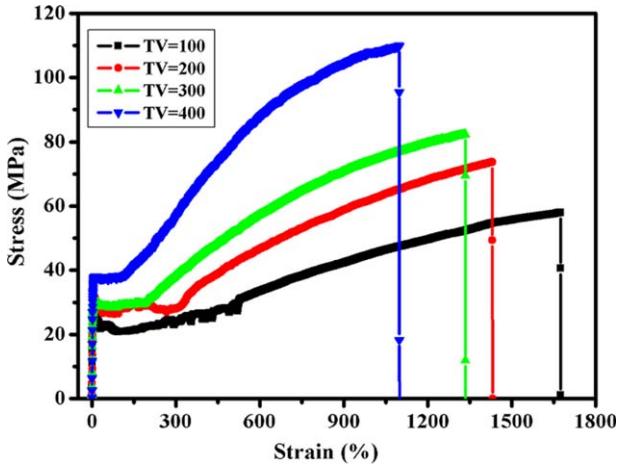

Figure 3. Typical stress–strain curves of melt-spun β-nucleated iPP fibers. [Color figure can be viewed in the online issue, which is available at wileyonlinelibrary.com.]

Two-Dimensional (2D) Wide Angle X-Ray Diffraction (WAXD) and Small Angle X-ray Scattering (SAXS) Measurement. The 2D-WAXD measurements were carried out using the U7B beam line of the National Synchrotron Radiation Laboratory (NSRL), University of Science and Technology of China, Hefei, China. The chosen X-ray wavelength λ was 0.154 nm and the distance from sample to detector was 375 mm. A Mar345 image-plate detector (by MAR Research Co. Ltd., Germany) was used to collect all 2D-WAXD images at room temperature.

The 2D-SAXS experiments were performed using a NanoSTAR-U (Bruker AXS Inc.) with a Cu Kα radiation source ($\lambda = 0.154$ nm). The generator was operated at 40 kV and 650μA. The 2D-SAXS intensity was collected with a 2D detector (Bruker Hi-star). The distance from sample to detector was 1058 mm. It should be noted that, for X-ray measurements, to obtain the maximum diffraction/scattering intensity, a bundle of melt-spun β-nucleated iPP fibers rather than a single fiber are characterized.

The orientation degree is calculated using Herman's orientation parameter f by the following equations[27]:

$$f = \frac{3\langle \cos^2 \varphi \rangle - 1}{2} \quad (1)$$

$$\langle \cos^2 \varphi \rangle = \frac{\int_0^{\pi/2} I(\varphi) \cos^2 \varphi \sin \varphi d\varphi}{\int_0^{\pi/2} I(\varphi) \sin \varphi d\varphi} \quad (2)$$

where φ is the angle between the normal of a given (hkl) crystal plane and the flow direction, and I is the intensity.

To get more insight into crystalline characteristics, one-dimensional wide-angle X-ray diffraction (1D-WAXD) curves are obtained from circularly integrated intensities of 2D-WAXD patterns, which are shown in Figure 6(a). Subsequently, through deconvoluting the peaks of 1D-WAXD curves [see Figure 6(b)], the overall crystallinity (X_c) is calculated according to the following equation:

$$X_c = \frac{\sum A_{\text{cryst}}}{\sum A_{\text{cryst}} + \sum A_{\text{amorp}}} \times 100\% \quad (3)$$

where A_{amorp} and A_{cryst} are the fitted area of the amorphous and crystalline peaks, respectively. The relative content of β-crystal ($K_{\beta\text{-WAXD}}$) is evaluated via the following equation[28]:

$$K_{\beta\text{-WAXD}} = \frac{A_{\beta(300)}}{A_{\alpha(110)} + A_{\alpha(040)} + A_{\alpha(130)} + A_{\beta(300)}} \times 100\% \quad (4)$$

here, $A_{\beta(300)}$ is the area of the (300) reflection peak; $A_{a(110)}$, $A_{a(040)}$, and $A_{a(130)}$ are the areas of the $(110)_\alpha$, $(040)_\alpha$, and $(130)_\alpha$ reflection peaks, respectively.

RESULTS

Tensile Properties

The typical stress–strain curves of melt-spun β-nucleated iPP fibers prepared upon different TVs are shown in Figure 3. In order to quantitatively estimate tensile properties, the average values of tensile properties, that is, ultimate tensile strength (σ), tensile modulus (E), elongation at break (ε), and strain energy density at break (W_b) are determined from the stress–strain curves and summarized in Table I.

Obviously, both tensile strength and modulus of melt-spun β-nucleated iPP fibers show substantial increases with increasing TV. For example, the tensile strength gradually improves from 62.7 MPa at TV = 100 cm/min to 109.0 MPa at TV = 400 cm/min; therefore, an increase of 74% is obtained. Correspondingly, the tensile modulus (calculated from the slope of the curves) of melt-spun β-nucleated iPP fibers enhances from 1.3 to 1.9 GPa. Clearly, the melt-spun β-nucleated iPP fiber prepared at higher TV (400 cm/min) has higher tensile strength and modulus compared with that prepared at lower one (100 cm/min). In addition, it is also seen that the elongation at break of melt-spun β-nucleated iPP fibers gradually decreases with increasing TV from 100 to 400 cm/min, which is attributed to the decrease of relative content of β-crystal, as shown later.

Furthermore, W_b, the total mechanical energy per unit volume consumed by the material when straining it to break is usually used as a measure for the toughness of a material.[29] Materials showing better toughness are generally those with higher W_b. It

Table I. Tensile Properties of Melt-Spun β-Nucleated iPP Fibers

TV (cm/min)	100	200	300	400
σ (MPa)	62.7 ± 0.1	83.1 ± 0.3	93.8 ± 0.3	109.0 ± 0.5
ε (%)	1704 ± 16	1404 ± 13	1207 ± 8	1110 ± 5
E (GPa)	1.3 ± 0.1	1.6 ± 0.2	1.8 ± 0.2	1.9 ± 0.4
W_b (MJ/m^3)	661 ± 19	713 ± 23	765 ± 26	853 ± 32

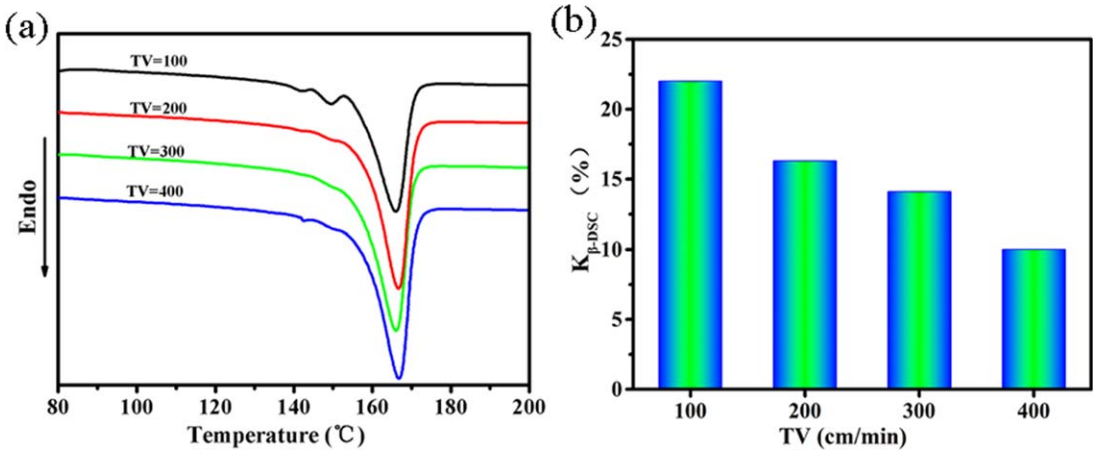

Figure 4. The DSC melting curves and the relative content of β-crystal ($K_{\beta\text{-DSC}}$) of melt-spun β-nucleated iPP fibers. [Color figure can be viewed in the online issue, which is available at wileyonlinelibrary.com.]

can be obtained by integrating the area under the stress-strain curves by the following equation[29]: $W_b = \int_0^{\varepsilon} \sigma d\varepsilon$. In this article, toughness is characterized according to this method. The corresponding data in Table I show a considerable increment in toughness with increasing TV. It can be concluded that the melt-spun β-nucleated iPP fibers prepared at higher TV successfully realize simultaneous enhancement of strength and toughness.

Since the microstructure is an important factor determining the tensile properties, a systematic characterization will be performed to furthermore explore the relationship between microstructure and tensile properties in the following section.

Thermal Behaviors

The melting curves for all melt-spun β-nucleated iPP fibers are shown in Figure 4(a). Clearly, for the melt-spun β-nucleated iPP fibers, there is a dominant peak around 167 °C, which is attributed to the melting of α-crystals. In addition, two additional melting peaks appear at around 144 °C and 150 °C, respectively. In our case, smaller peak located at 144 °C is believed to be the fusion of initial β-crystals, whereas endotherm located at 150 °C is related to the fusion of perfected or thickened lamellae formed by partial melting and recrystallization of initially formed crystals upon heating.[30] However, it can be obviously seen that the two small peaks become more indistinct with elevating TV, indicating that TV hinders the formation of β-crystal. In order to quantitatively estimate the variation of relative content of β-crystal (K_β) upon increasing TV, the $K_{\beta\text{-DSC}}$ is evaluated from the DSC melting curves according to the following equations:

$$K_{\beta\text{-DSC}} = \frac{X_\beta}{X_\alpha + X_\beta} \times 100\% \quad (5)$$

where X_α and X_β are the crystallinity of the α- and β-crystal, respectively, which can be calculated separately according to

$$X_i = \frac{\Delta H_i}{\Delta H_i^0} \quad (6)$$

where ΔH_i is the enthalpy of fusion of either α- or β-crystal and ΔH_i^0 is the enthalpy of fusion of 100% crystalline iPP of either α- or β-crystal. As reported elsewhere,[31] a value of 177 J/g for α-crystal and that of 168.5 J/g for β-crystal are used. The values of $K_{\beta\text{-DSC}}$ are presented in Figure 4(b). Obviously, $K_{\beta\text{-DSC}}$ value decreases with increasing TV, which are in agreement with our previous studies and its mechanism has been extensively discussed in detail.[32,33]

WAXD and SAXS Results

The 2D-WAXD and 2D-SAXS measurements were carried out to investigate the orientation and crystalline characteristics. The results are presented in Figure 5. As shown in 2D-WAXD patterns, the reflection arcs, respectively, originate from the α(110), β(300), α(040), α(130), α(111), and α(−131) from inner to

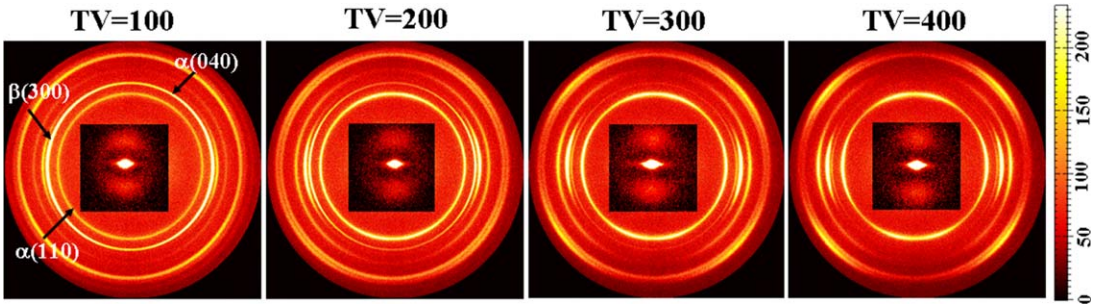

Figure 5. The 2D-WAXD patterns of melt-spun β-nucleated iPP fibers. The inset shows the corresponding 2D-SAXS patterns. The direction of stretching is vertical. [Color figure can be viewed in the online issue, which is available at wileyonlinelibrary.com.]

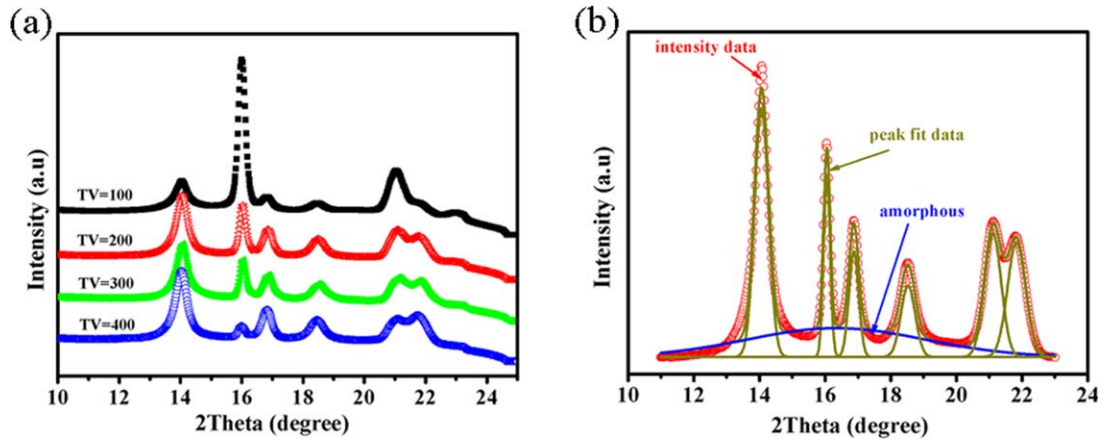

Figure 6. The 1D-WAXD profiles obtained from 2D-WAXD patterns of melt-spun β-nucleated iPP fibers and selected samples prepared at TV = 300 as a typical profile for calculating the crystallinity. [Color figure can be viewed in the online issue, which is available at wileyonlinelibrary.com.]

outer. In addition, it can be clearly seen that, the diffraction arcs become sharper in the diffraction patterns upon increasing TV, which is indicative of higher degree of orientation (f_{WAXD}) in the α-crystal [see Figure 7(a)]. The f_{WAXD} can be calculated using Herman's orientation parameter from the measured 2D-WAXD (040) reflection. According to 2D-SAXS images, all images show a pair of scattering spots at the meridional direction, originating from the lamellae perpendicular to the flow direction.[34] If TV is raised, the scattering intensity along the meridional direction obviously increases. This is also indicative of higher level of lamellar orientation (f_{SAXS}) [see Figure 7(a)]. Moreover, as shown in 2D-SAXS patterns, strong intensity streak in equatorial direction appears for all samples. This streak indicates the existence of shish-like structures containing fibrillar crystals.[34,35] In light of this, a conclusion can be safely obtained that shish-kebab structures will be formed, which can be explained based on the coil–stretch theory: as described in the Introduction section, elongational (stretching) flow is relatively strong compared with shear flow in melt-spinning, thus powerfully inducing the transformation from coiled chains to extended ones. When polymer melt is subjected to elongational flow, long coiled chains (longer than a critical length) of the polymer melt can be easily stretched to form the shish, on which the folded chain lamellae (kebabs) epitaxially grow.[36,37] Furthermore, the β-NA could lower the free energy barrier for the formation of shish or secondary nucleation,[38] which exactly promotes the formation of perpendicular lamellae.

According to eqs. (3) and (4), the crystallinity and the relative content of β-crystal can be calculated and the results are shown in Figure 7(b). From Figure 7(b), three important conclusions can be drawn: (1) on the whole, X_c generally keeps almost constant over the entire range of TV; (2) $K_{\beta\text{-WAXD}}$ gradually decreases with the increase of TV, indicating that increasing TV hinders the formation of β-crystal. It should be noted that there are some discrepancy between the results assessed by 2D-WAXD and those estimated by DSC as mentioned above. Such divergence can be explained as follows: some of the unstable β-crystals with thinner crystalline lamellae are transformed to α-crystals during the DSC heating program, which has been reported in other work.[39,40] In addition, since the 2D-WAXD is performed under room temperature, the β–α phase transformation can be excluded. However, the variation tendency of K_β calculated by 2D-WAXD is consistent with that of DSC result;

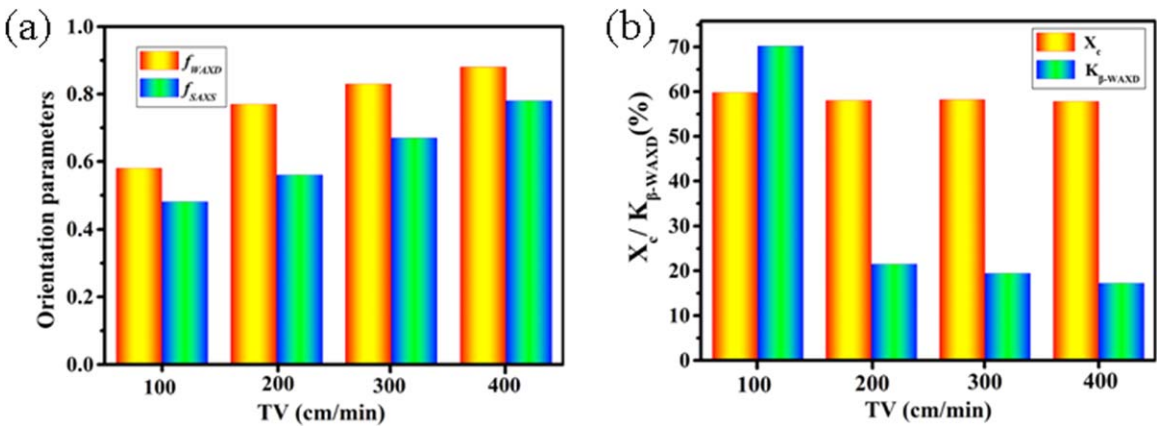

Figure 7. Orientation parameters and the crystallinity and relative content of β-crystal of melt-spun β-nucleated iPP fibers. [Color figure can be viewed in the online issue, which is available at wileyonlinelibrary.com.]

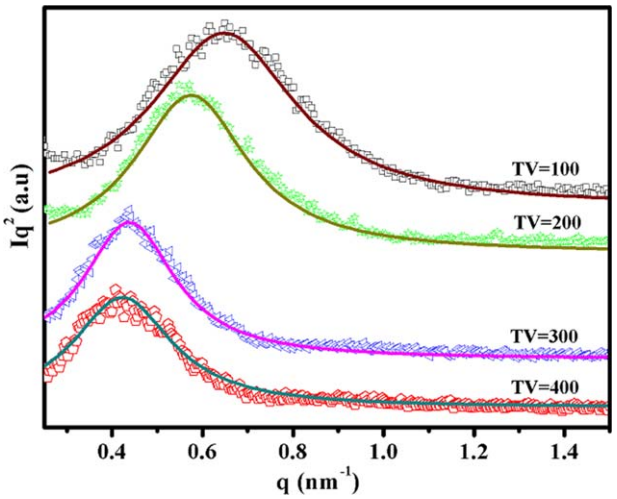

Figure 8. Lorentz-corrected 1D-SAXS intensity profiles. Solid lines are fitted data using the Lorentz method. [Color figure can be viewed in the online issue, which is available at wileyonlinelibrary.com.]

(3) both f_{WAXD} and f_{SAXS} elevate with increasing TV, suggesting that melt-spinning is indeed favorable for orientation. Note that f_{SAXS} is closely associated with the restriction of the neighboring shish-kebab structures, that is, denser shish-kebab structures lead to higher level of lamellar orientation.[41,42] In light of this, it is deduced that the amount of shish-kebabs formed in the samples prepared at higher TV (400 cm/min) is larger than that prepared at lower TV (100 cm/min), which can explain the dramatically enhanced tensile strength in this study.

With respect to lamellar arrangement of melt-spun β-nucleated iPP fibers, the long period (L), lamellae thickness (L_c), and crystallite size ($D_{(hkl)}$) are estimated. From the 1D-SAXS scattering peak position of q_m (see Figure 8), the long period, denoted as L_B, is calculated from the peak using Bragg's law($L_B=2\pi/q_m$). Meanwhile, the long period, denoted as L_{cor}, is also obtained from a correlation function given by[19]

$$K(z)=\frac{1}{2\pi^2}\int_0^\infty I(q)q^2\cos(qz)dq \quad (7)$$

where q is the scattering vector and is defined as $q=4\pi\sin\theta/\lambda$, θ denotes the Bragg angle. Figure 9(b) presents the curve of 1D electron density correlation function for the sample prepared at 200 cm/min. As indicated by the arrows, the curve gives various structural parameters,[43] for example, the crystalline long period (L_{cor}), lamellar thickness (L_c), and the thickness of rigid amorphous fraction (L_{ra}) between crystalline lamellae and amorphous phases. The amorphous thickness (L_a) can be obtained by subtracting L_c and $2L_{ra}$ from L_{cor}. In addition, the $D_{(hkl)}$ of each plane can be calculated from diffraction peaks of 1D-WAXD using the Scherrer equation[44]:

$$D_{(hkl)}=\frac{K\lambda}{\beta_{hkl}\cos\theta_{hkl}} \quad (8)$$

where $D_{(hkl)}$ is the crystallite diameter (hkl), λ is the wave length of the X-ray, K is crystallite shape factor ($K=0.89$), θ_{hkl} is the Bragg angle and β_{hkl} full width of the diffraction line at half-maximum intensity measured in radians. The calculated results are listed in Table II. Obviously, the long period (L_B and L_{cor}) and L_c show a significant increase with increasing TV, indicating that the crystalline structure becomes more perfection. However, the volume of rigid amorphous fraction (V_{RAF}), $D_{(040)}$ and $D_{(300)}$ decrease with elevating TV, which contribute to the enhancement of toughness for samples.

DISCUSSION

The experimental results show that both the tensile properties and microstructures depend on TV. The macroscopic properties of iPP depend on their microstructures. Therefore, it is desirable to investigate the relationships between the microstructures and mechanical properties of the samples. Usually, improved strength is at the expense of the deterioration of toughness; vice versa, the enhancement of toughness is at the sacrifice of strength.[46] However, the results reported in this study indicate that simultaneously reinforcing and toughening melt-spun β-nucleated iPP fibers has been successfully achieved. Hereinafter,

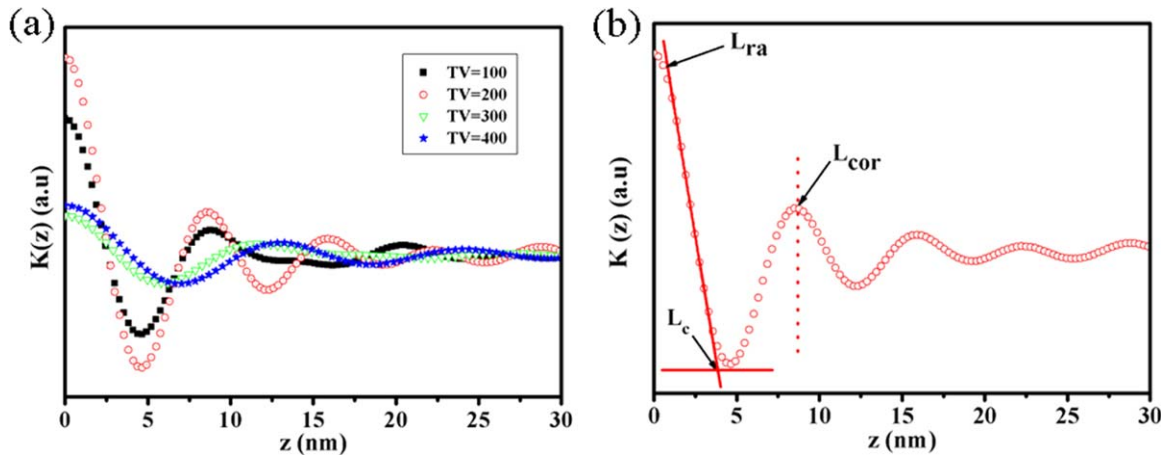

Figure 9. One dimensional correlation function $K(z)$ obtained from 1D-SAXS curves for samples and example of the period (L_{cor}), the thickness of rigid amorphous fraction (L_{ra}), and lamellar thickness (L_c) obtained from the correlation function. [Color figure can be viewed in the online issue, which is available at wileyonlinelibrary.com.]

Table II. The Long Periods (L_B and L_{cor}), Thicknesses of Crystalline Lamellae (L_c), and Amorphous Layer (L_a), Rigid Amorphous Fraction (L_{ra}), Volume Fraction of Rigid Amorphous Fraction (V_{RAF}) and Crystallite Size ($D_{(hkl)}$) of Melt-Spun β-Nucleated iPP Fibers

TV (cm/min)	100	200	300	400
L_B (nm)	9.72	10.91	14.34	14.72
L_{cor} (nm)	8.78	8.81	11.59	12.83
L_{ra} (nm)	1.31	1.20	1.58	1.70
L_c (nm)	3.76	3.77	4.80	5.73
L_a (nm)	2.40	2.64	3.63	3.70
V_{RAF} (%)	29.8	27.2	27.3	26.5
$D_{(040)}$ (nm)	26.2	25.1	24.6	23.1
$D_{(300)}$ (nm)	36.3	33.8	30.8	27.2

V_{RAF} is given by the ratio of $2L_{ra}$ to L according to Ref. 45.

we will study the relationships between microstructures and the improvement of tensile properties.

Mechanism for the Enhanced Tensile Strength

What causes such a dramatic increase in tensile strength of the melt-spun β-nucleated iPP fibers upon increasing TV? Generally speaking, tensile strength of semi-crystalline polymers is influenced by the following factors[18,25,46–49]: (1) total crystallinity; (2) orientation structure (i.e., shish-kebab); (3) orientation degree; and (4) crystalline morphology (lamellae thickness and crystalline forms). In the following section, the effect of these factors on tensile strength will be discussed in detail.

From Figure 7(b), the calculated results show almost the same X_c in all melt-spun β-nucleated iPP fibers. Thus, it can be deduced that X_c does not contribute to improvement of tensile strength. Therefore, the improvement of tensile strength is mainly governed by other factors. From a "microstructure–property" relation perspective, the enhancement of tensile strength can be explained based on shish-kebabs as a self-reinforced structure of iPP.[25,48,49] As shown in the 2D-SAXS results section, more shish-kebab structures will be formed in melt-spun β-nucleated iPP fibers prepared at higher TV, leading to the enhancement of tensile strength. Second, the orientation degree in semi-crystalline polymers (such as iPP) can remarkably enhance the tensile strength.[18,50] As shown in Figure 7(a), f_{WAXD} and f_{SAXS} of samples tend to increase with elevating TV, contributing to the improvement of tensile strength. Third, the larger L and L_c lead to the enhancement of molecular chain interactions, namely, elevating the fracture resistance. From Table II, it can be seen that the L and L_c gradually increase with TV. Thus, the increase of L and L_c must be an important factor for the improvement of tensile strength.[47] Finally, α-crystal content (crystalline forms) also plays an important role in the improvement of tensile strength for the films.[25,47] From Figures 4(b) and 7(b), it is easily found that K_β decreases with increasing TV, indicating the relative content of α-crystal increases at the cost of β-crystal. So it can be concluded that the large enhancements in tensile strength observed with increasing TV is as a result of the formation of shish-kebab structure, the progressive increase of the orientation degree, the increases of L and L_c as well as the enhancement of relative content of α-crystal.

Mechanism for the Enhanced Toughness

The increment of toughness derived from the stress-strain diagrams will be discussed in detail. It is widely reported that β-crystals in iPP are favorable and effective for toughening.[51,52] In our case, even though the K_β of melt-spun β-nucleated iPP fibers prepared at lower TV (100 cm/min) is higher than those prepared at larger TV (400 cm/min), they still exhibit not so high toughness (see Table I). The iPP fibers with high K_β even show rather lower toughness than those with low K_β. Therefore, we can conclude that the main factor for the improvement in toughness is not the variation of K_β. It should be noted that the elongation at break of melt-spun β-nucleated iPP fibers is proportional to the variation of K_β. As for the improved toughness, three main aspects will be considered in the following section: (1) The influence of decreased crystallite size ($D_{(hkl)}$). It has been proposed that the decreased $D_{(hkl)}$ lead to more tie molecules between the inter-lamellae, which would improve fracture toughness of iPP.[53,54] As listed in Table II, both $D_{(040)}$ and $D_{(300)}$ exhibit gradual decrease with elevating TV. Therefore, the decrease of $D_{(040)}$ and $D_{(300)}$ is one of the reason for improvement of toughness. (2) The role of crystalline structure. It has been reported that thin fiber-like crystallites will increase the number of spacing that can participate in energy dissipation, indicating the improvement of toughness.[50] Therefore, it can be naturally deduced that shish-like structures containing fibrillar crystals could also increase the number of spacing, leading to higher toughness. Since there are more shish-kebab structures for melt-spun β-nucleated iPP fibers prepared at higher TV than those prepared at lower TV, the former exhibit higher toughness than the latter. (3) The effect of rigid amorphous fraction (RAF). As well-known, there exists a RAF in numerous semi-crystalline polymers,[45] which is located at the interface between the crystalline and amorphous phases. The RAF is non-crystalline and originates from the continuation of the partially crystallized macromolecules across the phase boundaries. Moreover, it has been reported that the decrease of V_{RAF} leads to the enhanced molecular mobility in the amorphous phase for iPP samples, thus it promotes remarkable energy absorption.[55] According to aforementioned results of V_{RAF} listed in Table II, V_{RAF} shows a significant decrease with increasing TV, thus consuming a considerable amount of energy, that is, the notable enhancement of fracture toughness.

CONCLUSIONS

This study investigated the effect of microstructures on simultaneous strengthening and toughening of melt-spun β-nucleated iPP fibers. With increasing TV, tensile strength of melt-spun β-nucleated iPP fibers shows a 115.2% increment (from 62.7 to 135.0 MPa), in parallel with a considerable increment in toughness. Through thorough analysis of various structural characteristics, the notable improvement of tensile strength in melt-spun β-nucleated iPP fibers prepared at higher TV is ascribed to the combined effects of the formation of shish-kebab structure, the progressive increase of the orientation degree and lamellae thickness as well as the increment of relative content of α-

crystal. Meanwhile, compared with the melt-spun β-nucleated iPP fibers prepared at lower TV (100 cm/min), the decrease of crystal size and the formation of the more shish-like structures as well as the decrease of V_{RAF} could contribute to the improvement of toughness for those prepared at higher one (400 cm/min). It is worth stressing that the exploration herein gives more insights into the microstructures of β-nucleated iPP parts formed during intense stretching flow, which might open a promising door to optimizing the properties of melt-spun β-nucleated iPP fibers.

ACKNOWLEDGMENTS

The authors express thanks to the National Natural Science Foundation of China (51173171, 11172271), and HASTIT of Henan Province, State Key Laboratory of Materials Processing and Die & Mould Technology as well as The Key Laboratory of Polymer Processing Engineering, Ministry of Education, China. The authors would also like to thank Prof. Liangbin Li and Prof. Guoqiang Pan of University of Science and Technology of China for WAXD measurement at National Synchrotron Radiation Laboratory.

REFERENCES

1. Misra, S.; Lu, F. M.; Spruiell, J.; Richeson, G. *J. Appl. Polym. Sci.* **1995**, *56*, 1761.
2. Bond, E. B.; Spruiell, J. E. *J. Appl. Polym. Sci.* **2001**, *82*, 3223.
3. Ščudla, J.; Raab, M.; Eichhorn, K. J.; Strachota, A. *Polymer* **2003**, *44*, 4655.
4. Kotek, J.; Kelnar, I.; Baldrian, J.; Raab, M. *Eur. Polym. J.* **2004**, *40*, 679.
5. Lotz, B.; Wittmann, J.; Lovinger, A. *Polymer* **1996**, *37*, 4979.
6. Qiu, J.; Wang, Z. G.; Yang, L.; Zhao, J. C.; Niu, Y. H.; Hsiao, B. S. *Polymer* **2007**, *48*, 6934.
7. Fujiwara, Y. *Colloid. Polym. Sci.* **1975**, *253*, 273.
8. Ellis, G.; Gomez, M.; Marco, C. *J. Macromol. Sci., Part B* **2005**, *43*, 191.
9. Byelov, D.; Panine, P.; Remerie, K.; Biemond, E.; Alfonso, G. C.; de Jeu, W. H. *Polymer* **2008**, *49*, 3076.
10. Liu, Z. Z.; Liu, X. H.; Zheng, G. Q.; Dai, K.; Liu, C. T.; Shen, C. Y. *J. Mater. Sci.* **2015**, *50*, 599.
11. Varga, J. *J. Therm. Anal. Calorim.* **1989**, *35*, 1891.
12. Lotz, B. *Polymer* **1998**, *39*, 4561.
13. Zhou, J. J.; Liu, J. G.; Yan, S. K.; Dong, J. Y.; Li, L.; Chan, C. M.; Schultz, J. M. *Polymer* **2005**, *46*, 4077.
14. Xiao, W. C.; Wu, P. Y.; Feng, J. C.; Yao, R. Y. *J. Appl. Polym. Sci.* **2009**, *111*, 1076.
15. Luo, F.; Geng, C. Z.; Wang, K.; Deng, H.; Chen, F.; Fu, Q.; Na, B. *Macromolecules* **2009**, *42*, 9325.
16. Varga, J.; Tóth, F. S. *Die Makromol. Chem.* **1991**, *188*, 11.
17. Abuzaina, F. M.; Fitz, B. D.; Andjelic, S.; Jamiolkowski, D. D. *Polymer* **2002**, *43*, 4699.
18. Hou, Z. C.; Wang, K.; Zhao, P.; Zhang, Q.; Yang, C. Y.; Chen, D. Q.; Du, R. N.; Fu, Q. *Polymer* **2008**, *49*, 3582.
19. Strobl, G., The Physics of Polymers: Concepts for Understanding Their Structure and Behavior; Springer: Berlin, Germany, **1997**; p 408.
20. Carothers, W. H.; Hill, J. W. *J. Am. Chem. Soc.* **1932**, *54*, 1579.
21. Sheehan, W.; Cole, T. *J. Appl. Polym. Sci.* **1964**, *8*, 2359.
22. Lu, F. M.; Spruiell, J. E. *J. Appl. Polym. Sci.* **1987**, *34*, 1521.
23. Lu, F. M.; Spruiell, J. E. *J. Appl. Polym. Sci.* **1993**, *49*, 623.
24. Spruiell, J. E.; Lu, F. M.; Ding, Z.; Richeson, G. *J. Appl. Polym. Sci.* **1996**, *62*, 1965.
25. Gao, Y.; Ren, K.; Ning, N. Y.; Fu, Q.; Wang, K.; Zhang, Q. *Polymer* **2012**, *53*, 2792.
26. Xiao, W. C.; Wu, P. Y.; Feng, J. C. *J. Appl. Polym. Sci.* **2008**, *108*, 3370.
27. Picken, S. J.; Aerts, J.; Visser, R.; Northolt, M. G. *Macromolecules* **1990**, *23*, 3849.
28. Turner-Jones, A. *Die Makromol. Chem.* **1964**, *71*, 1.
29. Van Vlack, L. H. Elements of materials science and engineering, Addison-Wesley: New York, **1989**.
30. Cho, K.; Nabi Saheb, D.; Yang, H.; Kang, B. I.; Kim, J.; Lee, S. S. *Polymer* **2003**, *44*, 4053.
31. Li, J. X.; Cheung, W. L.; Jia, D. *Polymer* **1999**, *40*, 1219.
32. Li, S. W.; Zheng, G. Q.; Jia, Z. H.; Zhang, Z. F.; Liu, C. T.; Chen, J. B.; Li, Q.; Shen, C. Y.; Peng, X. F. *J. Macromol. Sci., Part B* **2012**, *51*, 828.
33. Zheng, G. Q.; Li, S. W.; Zhang, X. L.; Liu, C. T.; Dai, K.; Chen, J. B.; Li, Q.; Peng, X. F.; Shen, C. Y. *Polym. Int.* **2011**, *60*, 1016.
34. Jiang, Z.; Tang, Y.; Rieger, J.; Enderle, H. F.; Lilge, D.; Roth, S. V.; Gehrke, R.; Wu, Z.; Li, Z.; Li, X. *Eur. Polym. J.* **2010**, *46*, 1866.
35. Murthy, N.; Bednarczyk, C.; Moore, R.; Grubb, D. *J. Polym. Sci., Part B: Polym. Phys.* **1996**, *34*, 821.
36. Pope, D.; Keller, A. *Colloid. Polym. Sci.* **1978**, *256*, 751.
37. Somani, R. H.; Hsiao, B. S.; Nogales, A.; Fruitwala, H.; Srinivas, S.; Tsou, A. H. *Macromolecules* **2001**, *34*, 5902.
38. Liu, X. H.; Dai, K.; Zheng, G. Q.; Liu, C. T.; Schubert, D. W.; Shen, C. Y. *Ind. Eng. Chem. Res.* **2013**, *52*, 11996.
39. Zhou, G. E.; He, Z. Q.; Yu, J. M.; Han, Z. W.; Shi, G. Y. *Die Makromol. Chem.* **1986**, *187*, 633.
40. Yuan, Q.; Jiang, W.; An, L. *J. Colloid. Polym. Sci.* **2004**, *282*, 1236.
41. Keller, A. *Polymer* **1962**, *3*, 393.
42. Schrauwen, B.; Breemen, L. V.; Spoelstra, A.; Govaert, L.; Peters, G.; Meijer, H. *Macromolecules* **2004**, *37*, 8618.
43. Strobl, G.; Schneider, M. *J. Polym. Sci., Part B: Polym. Phys. Ed.* **1980**, *18*, 1343.
44. Klung, H.; Alexander, L., X-ray Diffraction Procedures; Wiley: New York, **1974**; Vol. *1*, p 974.
45. Bai, H. W.; Luo, F.; Zhou, T. N.; Deng, H.; Wang, K.; Fu, Q. *Polymer* **2011**, *52*, 2351.
46. Chen, Y. H.; Zhong, G. J.; Wang, Y.; Li, Z. M.; Li, L. *Macromolecules* **2009**, *42*, 4343.

47. Pukánszky, B.; Mudra, I.; Staniek, P. *J. Vinyl. Technol.* **2004**, *3*, 53.
48. Mai, F.; Pan, D. D.; Gao, X.; Yao, M. J.; Deng, H.; Wang, K.; Chen, F.; Fu, Q. *Polym. Int.* **2011**, *60*, 1646.
49. Su, R.; Wang, K.; Ning, N. Y.; Chen, F.; Zhang, Q.; Wang, C. Y.; Fu, Q.; Na, B. *Compos. Sci. Technol.* **2010**, *70*, 685.
50. Zhao, P.; Wang, K.; Yang, H.; Zhang, Q.; Du, R. N.; Fu, Q. *Polymer* **2007**, *48*, 5688.
51. Fujiyama, M. *Int. Polym. Process.* **1995**, *10*, 172.
52. Fujiyama, M. *Int. Polym. Process.* **1998**, *13*, 291.
53. Greco, R.; Ragosta, G. *J. Mater. Sci.* **1988**, *23*, 4171.
54. Shi, S. Y.; Pan, Y. M.; Lu, B.; Zheng, G. Q.; Liu, C. T.; Dai, K.; Shen, C. Y. *Polymer* **2013**, *54*, 6843.
55. Na, B.; Li, Z. M.; Lv, R. H.; Zou, S. F. *Polym. Eng. Sci.* **2012**, *52*, 893.